Spin-induced symmetry breaking in orbitally ordered $NiCr_2O_4$ and $CuCr_2O_4$

Matthew R. Suchomel,[*] Daniel P. Shoemaker,[†] and Lynn Ribaud[‡]
X-Ray Science Division and Material Science Division Argonne National Laboratory, Argonne, Illinois 60439, USA

Moureen C. Kemei[§] and Ram Seshadri[‖]
Materials Department and Materials Research Laboratory University of California, Santa Barbara, California 93106, USA
(Received 25 June 2012; revised manuscript received 20 July 2012; published 6 August 2012)

At room temperature, the normal oxide spinels $NiCr_2O_4$ and $CuCr_2O_4$ are tetragonally distorted and crystallize in the $I4_1/amd$ space group due to cooperative Jahn-Teller ordering driven by the orbital degeneracy of tetrahedral Ni^{2+} (t_2^4) and Cu^{2+} (t_2^5). Upon cooling, these compounds undergo magnetic ordering transitions; interactions are somewhat frustrated for $NiCr_2O_4$ but not for $CuCr_2O_4$. We employ variable-temperature high-resolution synchrotron x-ray powder diffraction to establish that at the magnetic ordering temperatures there are further structural changes, which result in both compounds distorting to an orthorhombic structure consistent with the $Fddd$ space group. $NiCr_2O_4$ exhibits additional distortion, likely within the same space group, at a yet-lower transition temperature of $T = 30$ K. The tetragonal to orthorhombic structural transition in these compounds appears to primarily involve changes in NiO_4 and CuO_4 tetrahedra.

DOI: 10.1103/PhysRevB.86.054406 PACS number(s): 61.50.Ks, 75.47.Lx, 75.50.Gg

I. INTRODUCTION

Strong coupling between spin, lattice, and orbital degrees of freedom in functional transition metal oxide compounds results in rich behavior such as the tendency for cooperative Jahn-Teller[1] and spin-Peierls distortions.[2] Such coupling between the different degrees of freedom enables multifunctionality as observed in multiferroics $RMnO_3$(R = heavy rare-earth metal).[3,4] In these systems, manipulation of one property can influence another, exemplified by the electric field control of magnetic polarization in $HoMnO_3$.[5] Seeking out such strong links between distinct degrees of freedom represents a powerful strategy in the search for new multifunctional systems, and affords unique opportunities for a deeper understanding of these interactions.[6,7]

One such frequently studied interaction is magnetostructural coupling in geometrically frustrated antiferromagnets[8,9] where a structural distortion lifts the large ground state degeneracy allowing long-range magnetic order.[10,11] However, frustration-driven magnetostructural coupling is not expected in the ferrimagnetic spinels with the formula ACr_2O_4 where A is a magnetic cation. This is a consequence of the magnetic A-O-Cr^{3+} interaction usually being collectively stronger than the frustrated interactions between the Cr^{3+}. Furthermore, Jahn-Teller activity of the A site cation can cause tetragonal distortions that should further alleviate frustration in the Cr^{3+} sublattice. Nonetheless, previous structural, thermodynamic, and magnetic studies of $NiCr_2O_4$ (Refs. 12 and 13) report a coupled magnetic and structural transition, and infrared spectroscopy measurements suggest concurrent magnetic and structural transitions in $CuCr_2O_4$.[14]

Structural transitions at the magnetic ordering temperatures have been observed in numerous transition metal oxide antiferromagnets such as Cr_2O_3,[15] MnO,[16,17] FeO,[16,17] CoO,[16,17] and NiO.[16,17] Cubic to rhombohedral transformations are found in MnO, FeO, and NiO, while CoO undergoes a cubic to tetragonal transition. The rhombohedral lattice constants of Cr_2O_3 change at its antiferromagnetic ordering temperature. Two mechanisms of magnetostructural coupling have been suggested in these compounds based on neutron and x-ray diffraction measurements. Li has suggested that magnetostructural coupling in NiO, MnO, CoO, and FeO is driven by magnetostriction,[18] where anisotropy arises from the selection of a magnetic ordering axis and drives the magnetocrystalline deformation. Smart and Greenwald alternatively proposed that distortions in the above binary oxides are caused by exchange striction, which is the displacement of interacting ions to strengthen exchange coupling thus modifying the underlying lattice.[19] The relations between crystal distortions and exchange interactions are challenging to identify. For example, it is difficult to find a unique solution to certain magnetic scattering patterns.[17,18]

Here, we determine the low-temperature structures of $NiCr_2O_4$ and $CuCr_2O_4$ across the transitions associated with magnetic ordering using high-resolution synchrotron powder x-ray diffraction. These compounds are fully ordered and stoichiometric normal cubic spinels with the space group $Fd\bar{3}m$ at temperatures above 320 K (Refs. 20 and 21) for $NiCr_2O_4$ and 853 K (Refs. 21 and 22) for $CuCr_2O_4$.[23] Cr^{3+} $3d^3$ preferentially populates the octahedral sites because of the strong crystal field stabilization of the half occupied nondegenerate t_{2g} states and empty e_g states, while Ni^{2+} $3d^8$ and Cu^{2+} $3d^9$ are found on the tetrahedral sites.[1] The tetrahedral crystal field around Ni^{2+} $3d^8$ and Cu^{2+} $3d^9$ in the cubic phase results in fully occupied low-energy e levels and triply degenerate t_2 levels, rendering this structure potentially unstable.[24,25] A cooperative lattice distortion—from cubic to tetragonal symmetry—lifts the orbital degeneracy in $NiCr_2O_4$ at 320 K (Refs. 13,20 and 26) and in $CuCr_2O_4$ at 853 K.[22,26] There had been a debate in the literature concerning the ambient temperature structure of $CuCr_2O_4$. Using neutron diffraction data, Prince postulated that the noncentrosymmetric space group $I\bar{4}2d$ was a better structural fit than $I4_1/amd$.[27] More recently, Dollase and O'Neill showed no statistically significant advantage to using the $I\bar{4}2d$ structural model over the centrosymmetric structure $I4_1/amd$.[28] In the tetragonal structure of $CuCr_2O_4$, CuO_4 tetrahedra are compressed toward a square planar

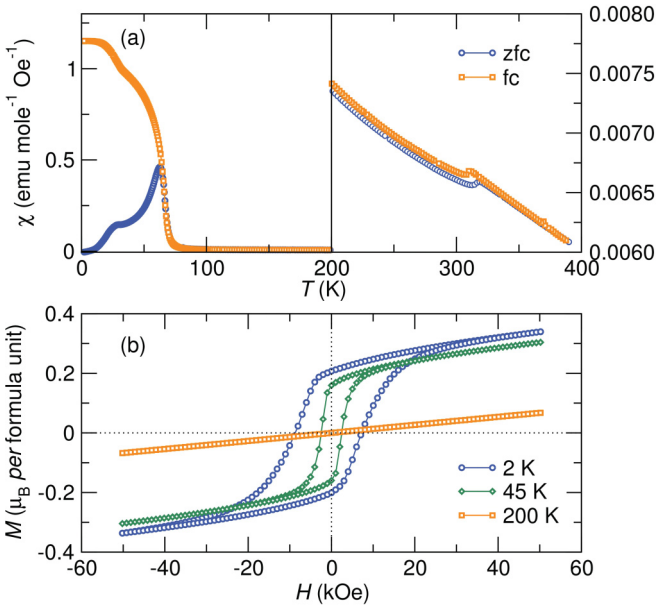

FIG. 1. (Color online) Magnetic measurements of the spinel $NiCr_2O_4$. (a) Zero field cooled and field cooled temperature-dependent magnetic susceptibility measured under a 1000 Oe dc field show three anomalies at 310, 65, and 30 K. $NiCr_2O_4$ displays little change in the magnetism at 310 K, and is seen to order ferrimagnetically at 65 K, with an additional change in the magnetic structure at 30 K. (b) The isothermal field-dependent magnetization measured above the magnetic ordering temperature shows paramagnetic behavior. At 2 K, the coercive field and saturation magnetization are significantly larger than what is observed at 45 K.

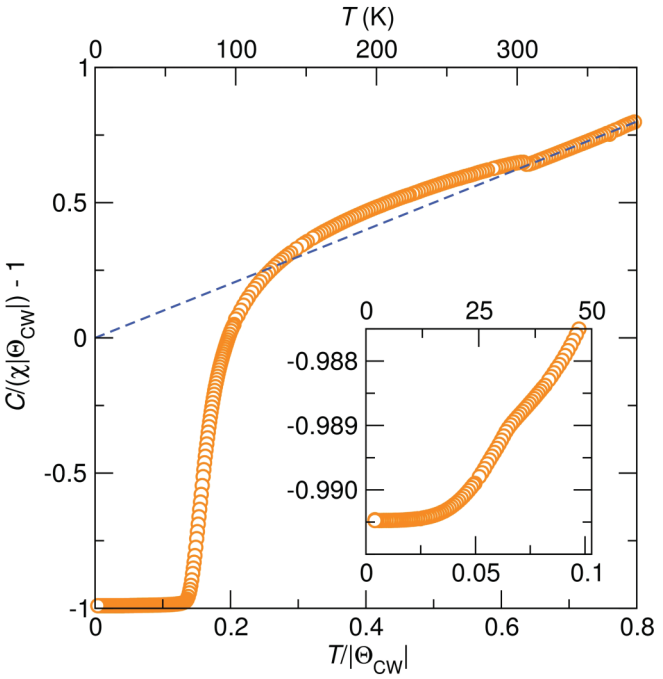

FIG. 2. (Color online) Normalized inverse magnetic susceptibility of $NiCr_2O_4$ showing ideal Curie-Weiss paramagnetism above 310 K. Weak compensated interactions arise at 310 K and persist to about 65 K below which strong uncompensated interactions dominate. The subtle magnetic transition at 30 K is shown in the inset.

configuration, thus lifting orbital degeneracy.[1] The tetragonal structure of $NiCr_2O_4$ is known to crystallize in the space group $I4_1/amd$ with elongated NiO_4 tetrahedra.[29] Previous work has also shown further distortion of tetragonal $NiCr_2O_4$ to an orthorhombic phase, which occurs at the magnetic transition temperature $T_N = 60$ K and has been observed in thermodynamic, x-ray diffraction, and magnetic studies.[12,13]

Noncollinear ferrimagnetism that is not described by the Néel model is observed in both $NiCr_2O_4$ and $CuCr_2O_4$. Tomiyasu and Kagomiya describe a magnetic structure comprising of a ferrimagnetic component and an antiferromagnetic component in $NiCr_2O_4$.[13,30] These authors used neutron scattering to show that the antiferromagnetic component orders at $T = 31$ K while the ferrimagnetic component orders at $T = 74$ K. A saturation magnetization moment of 0.3 μ_B per formula unit has been reported for $NiCr_2O_4$.[30] Neutron scattering studies on $CuCr_2O_4$ suggest a magnetic structure comprising of two canted Cr^{3+} sublattices with a net moment, and a Cu^{2+} sublattice that couples antiferromagnetically to the net moment of the Cr^{3+} sublattices below $T_N = 135$ K.[21,26,27] The magnetic moment of $CuCr_2O_4$ in this structure is 0.5 μ_B per formula unit.

Given this prior evidence of concurrent magnetic and structural transitions in $NiCr_2O_4$ (Refs. 12 and 13) and $CuCr_2O_4$,[14] there is a clear need for further exploration of these compounds. In this study, we employ high-resolution temperature-dependent powder x-ray diffraction, magnetic susceptibility, and heat capacity measurements to investigate

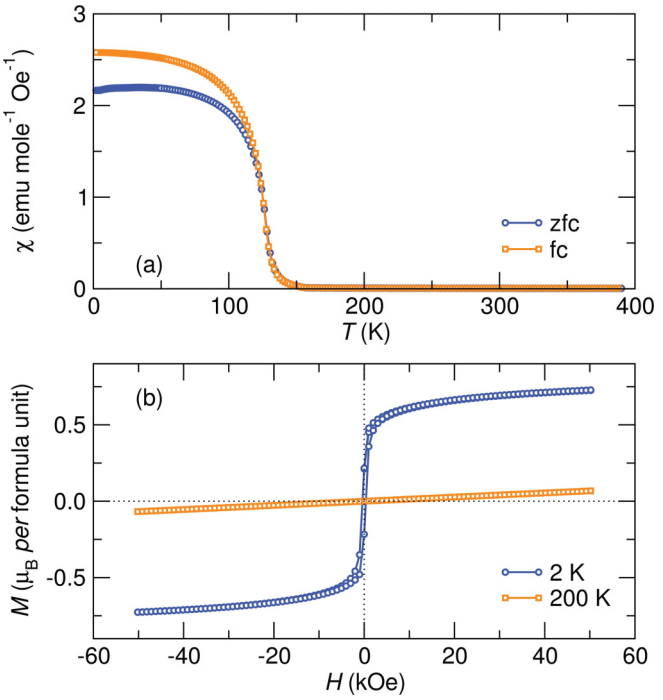

FIG. 3. (Color online) Magnetic measurements of the spinel $CuCr_2O_4$. (a) Magnetic susceptibility as a function of temperature under a 1000 Oe dc field shows an increase in susceptibility at the magnetic ordering temperature ≈130 K in both zero field cooled and field cooled measurements. This is a paramagnetic to ferrimagnetic transition. (b) Isothermal field-dependent magnetization measured above (200 K) and below (2 K) the magnetic ordering temperature.

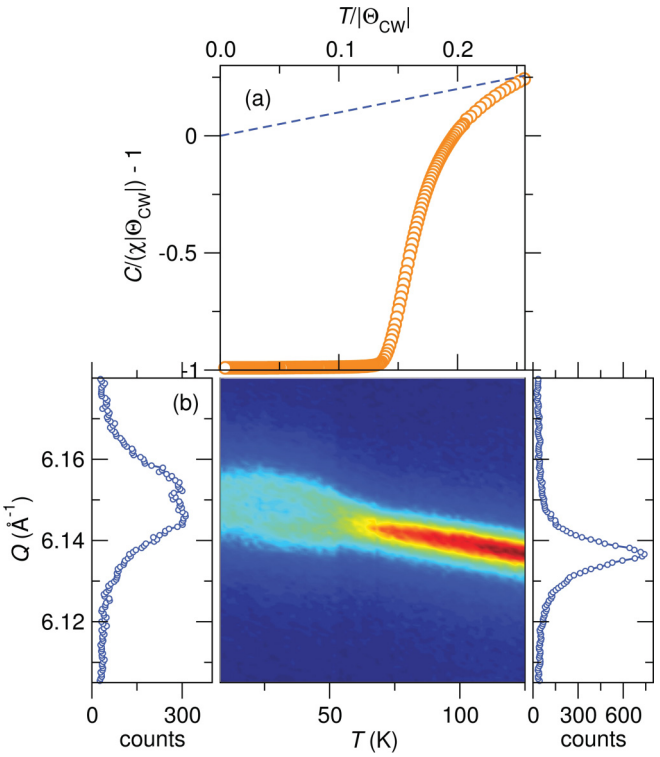

FIG. 4. (Color online) Magnetostructural coupling in $NiCr_2O_4$. (a) $NiCr_2O_4$ orders ferrimagnetically at $T_N = 65$ K, where the normalized inverse magnetic susceptibility deviates negatively from ideal CW paramagnetic behavior. (b) A structural transition occurs at the ferrimagnetic ordering temperature seen from the splitting of the tetragonal 440 diffraction peak into 080 and 800 orthorhombic peaks. Below 30 K, a subtle peak narrowing and intensity change is coincident with anomalies in magnetic and specific heat measurements. Diffraction patterns at 125 and 7 K are shown to the right and left of the central panel. During this structural transition, the 440 reflection splits in the Q range 10^{-2}Å, well within the instrumental resolution of 10^{-4}Å.

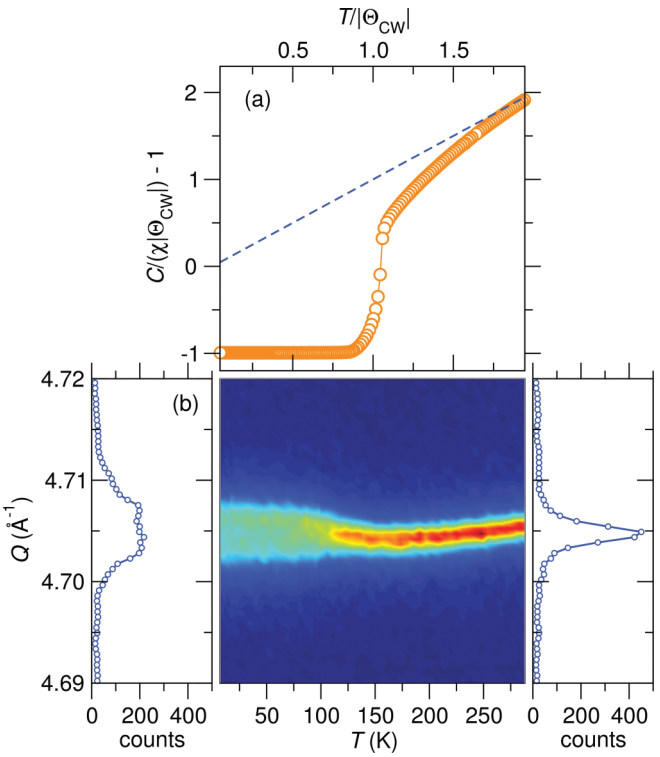

FIG. 5. (Color online) Magnetostructural coupling in $CuCr_2O_4$. (a) Long-range ferrimagnetic order occurs at $T_N = 130$ K in $CuCr_2O_4$ where the normalized inverse magnetic susceptibility of $CuCr_2O_4$ deviates negatively from ideal CW behavior. (b) Concurrent with the onset of magnetic order is a structural transition seen in the splitting of the tetragonal 322 reflection into orthorhombic 206 and 260 reflections. Diffraction patterns at 288 and 7 K are shown to the right and left of the central plot, respectively. This structural distortion results in reflection splitting in the Q range 10^{-2}Å, well within the instrumental resolution of 10^{-4}Å.

magnetostructural coupling in $NiCr_2O_4$ and $CuCr_2O_4$. This is the first observation by x-ray powder diffraction of the tetragonal to orthorhombic structural distortion of $CuCr_2O_4$ at the ferrimagnetic ordering temperature. We also reveal x-ray diffraction evidence of further symmetry lowering in orthorhombic $NiCr_2O_4$ at the second magnetic transition $T = 30$ K. These results affirm that strong magnetostructural coupling can also occur in spinels that are not expected to be frustrated. This understanding of coupling between spin and lattice degrees of freedom in $NiCr_2O_4$ and $CuCr_2O_4$ suggests that these compounds are promising magnetodielectrics, and provides considerable motivation for further investigation of magnetostructural coupling in related spinel compounds.

II. METHODS

$NiCr_2O_4$ was prepared by dissolving stoichiometric amounts of $Ni(NO_3)_2{\cdot}6H_2O$ and $Cr(NO_3)_3{\cdot}9H_2O$ in deionized water. The nitrate solution was heated to evaporate the solvent, leaving a precipitate that was ground and calcined at 1000° C for 24 hours. A dark green powder of $NiCr_2O_4$ was obtained. Black shiny single crystals of $CuCr_2O_4$ were prepared following the flux method described by Ye *et al.*[22] $K_2Cr_2O_7$ was used as a reactive flux that partly decomposes to Cr_2O_3 at ~ 700 K. Ye *et al.* propose that the reduction of Cr^{6+} into Cr^{3+} plays an important role in stabilizing the oxidation state of Cu^{2+} during the synthesis of $CuCr_2O_4$.[22] $K_2Cr_2O_7$ acts both as a flux and a source of Cr_2O_3. A 20 g mixture of 17.8% mass CuO (Sigma Aldrich 98%) and 82.2% mass $K_2Cr_2O_7$ (Fisher 99%) with 0.2 g Bi_2O_3 as a second flux was prepared. The mixture was ground using an agate mortar and pestle, placed in a covered platinum crucible, heated to 800° C with a ramp of 100°C/h, held for 24 h, and slowly cooled to ambient temperature at 15°C/h. After the reaction, black crystals of $CuCr_2O_4$ were collected and washed in boiling water. It should be noted that more conventional solid state preparation yielded samples with significantly broader linewidths in the synchrotron x-ray diffraction profile, potentially obscuring the ability to fully characterize the low-temperature structure. High-resolution ($\Delta Q/Q \leqslant 2 \times 10^{-4}$) synchrotron x-ray powder diffraction data were recorded on beamline 11-BM at the Advanced Photon Source (APS), Argonne National Laboratory.[31] Scans were collected using a 2Θ step size of 0.001° with $\lambda = 0.413441$ Å for $NiCr_2O_4$ and $\lambda = 0.413263$ Å for $CuCr_2O_4$ in a closed-flow helium cryostat over the temperature range 7–300 K. The sample was in direct contact with the helium

TABLE I. Structural parameters of $NiCr_2O_4$ and $CuCr_2O_4$ obtained from Rietveld refinement of high-resolution synchrotron x-ray diffraction data collected at temperatures above and below the orthorhombic distortion of both compounds.

	$NiCr_2O_4$		$CuCr_2O_4$	
	Orthorhombic	Tetragonal	Orthorhombic	Tetragonal
T	10 K	100 K	10 K	298 K
Space group	$Fddd$	$I4_1/amd$	$Fddd$	$I4_1/amd$
Setting	origin 2	origin 2	origin 2	origin 2
Z	8	4	8	4
a (Å)	8.18139(5)	5.79029(2)	7.71271(2)	6.03277(1)
b (Å)	8.16699(4)	5.79029(2)	8.53611(2)	6.03277(1)
c (Å)	8.56786(4)	8.54639(4)	8.54357(2)	7.78128(1)
Vol/Z (Å^3)	71.5601(6)	71.6346(4)	70.3098(3)	70.7986(2)
Ni/Cu	8a (1/8, 1/8 1/8)	4a (0, 1/4, 3/8)	8a (1/8, 1/8 1/8)	4a (0, 1/4, 3/8)
U_{iso} (10^2 Å^2)	0.01(1)	0.13(1)	0.08(1)	0.67(1)
Cr	16d (1/2, 1/2, 1/2)	8d (0,0,0)	16d (1/2, 1/2, 1/2)	8d (0,0,0)
U_{iso} (10^2 Å^2)	0.01(1)	0.019(1)	0.07(1)	0.29(1)
O	32h (x,y,z)	16h ($0,y,z$)	32h (x,y,z)	16h ($0,y,z$)
	x 0.2561(2)	x 0	0.2446(1)	0
	y 0.2589(2)	y 0.5152(2)	0.2675(2)	0.5364(1)
	z 0.2683(1)	z 0.2322(2)	0.2675(2)	0.2526(1)
U_{iso} (10^2 Å^2)	0.03(2)	0.16(2)	0.06(2)	0.55(1)
χ^2	3.85	4.15	2.31	3.84
R_p (%)	6.25	7.06	7.50	8.96
R_{wp} (%)	8.39	9.41	8.39	6.65

exchange gas during data collection, and was spun at 5 Hz to improve powder averaging. Structural models of $NiCr_2O_4$ and $CuCr_2O_4$ were fit to the diffraction data using the Rietveld refinement method as implemented in the EXPGUI/GSAS software program.[32,33] Crystal structures were visualized using the program VESTA.[34] In each composition, a single small impurity phase was observed in the powder diffraction data, and quantitatively fit using the Rietveld method. The $NiCr_2O_4$ sample was determined to have a 0.5 wt% of Cr_2O_3, and the $CuCr_2O_4$ sample a 1.1 wt% CuO impurity.

Magnetic susceptibility measurements on powder samples were performed using a Quantum Design MPMS 5XL superconducting quantum interference device (SQUID) magnetometer. Heat capacity measurements were collected on pellets of 50% mass silver and 50% mass sample using a Quantum Design Physical Properties Measurement System. The pellets were prepared by grinding equal amounts of silver and sample in an agate mortar and pestle followed by pressing at ~330 MPa. Apiezon N grease was used to enhance thermal coupling between the sample and the stage. The heat capacity of the Apiezon N grease and silver were collected separately and subtracted from the measured heat capacity.

III. RESULTS AND DISCUSSION

A. Magnetism

Three magnetic transitions are observed in the temperature-dependent magnetic susceptibility of $NiCr_2O_4$ (Fig. 1). A high-temperature transition occurs at 310 K where cooperative Jahn-Teller distortions lift the orbital degeneracy in $NiCr_2O_4$ and lower the structural symmetry from cubic ($Fd\bar{3}m$) to tetragonal ($I4_1/amd$) [Fig. 1(a)]. Weak, compensated magnetic interactions occur at 310 K, as illustrated by the scaled inverse susceptibility of $NiCr_2O_4$ (Fig. 2). The scaling is carried out by recasting the Curie-Weiss equation using[35]

$$\frac{C}{\chi|\Theta_{CW}|} + \mathrm{sgn}(\Theta_{CW}) = \frac{T}{|\Theta_{CW}|}. \quad (1)$$

The linear dependence of the magnetization on the applied field at 200 K [Fig. 1(b)] suggests that $NiCr_2O_4$ is mainly paramagnetic down to 65 K where there is a transition to a ferrimagnetic state [Fig. 1(a)]. The normalized inverse magnetic susceptibility trace shows the development of strong uncompensated magnetic correlations at 65 K (Fig. 2). A small coercive field and saturation magnetization is observed in the field-dependent magnetization of $NiCr_2O_4$ at 45 K [Fig. 1(b)] in agreement with the onset of ferrimagnetic order. Tomiyasu and Kagomiya attribute the magnetic transition at 65 K in $NiCr_2O_4$ to the ordering of the longitudinal ferrimagnetic component of $NiCr_2O_4$.[30] At 30 K, another anomaly is observed in both zero field cooled (ZFC) and field cooled (FC) measurements of the temperature-dependent magnetic susceptibility [Fig. 1(a)] as well as in the scaled inverse susceptibility (Fig. 2) of $NiCr_2O_4$. Below 30 K, an increase in the coercive field and the saturation magnetization of $NiCr_2O_4$ is observed [Fig. 1(b)]. Previous neutron diffraction measurements of $NiCr_2O_4$ attribute this anomaly to the ordering of the antiferromagnetic component of $NiCr_2O_4$.[30]

The temperature-dependent magnetic susceptibility of $CuCr_2O_4$ shows a rapid increase at 130 K where there is a paramagnetic to ferrimagnetic transition [Fig. 3(a)]. The ZFC susceptibility exhibits a reduced low-temperature saturation value when compared to the FC susceptibility data illustrating domain behavior. A linear dependence of magnetization with applied field occurs before the onset of magnetic order while a magnetization trace with a coercive field of 380 Oe and

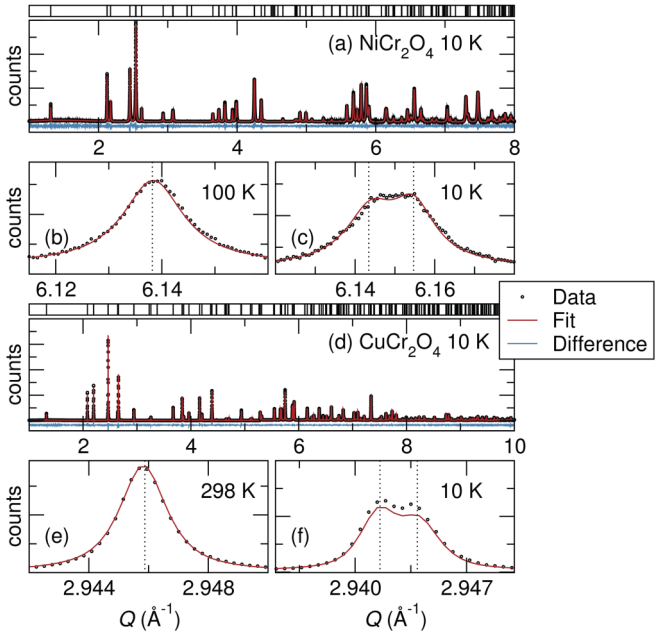

FIG. 6. (Color online) High-resolution synchrotron powder x-ray diffraction of $NiCr_2O_4$ and $CuCr_2O_4$. (a) The low-temperature diffraction pattern of $NiCr_2O_4$ is indexed to the orthorhombic space group $Fddd$. The lowering of average crystal symmetry in $NiCr_2O_4$ from tetragonal to orthorhombic symmetry is illustrated by the splitting of the (b) tetragonal (440) reflection into (c) orthorhombic 800 and 080 reflections. (d) Like $NiCr_2O_4$, the low-temperature diffraction data of $CuCr_2O_4$ is indexed to the orthorhombic space group $Fddd$ which is evident in the splitting of (e) (220) tetragonal reflections into (f) 004 and 040 orthorhombic reflections. Structural models are fit to the x-ray powder diffraction patterns using the Rietveld refinement method.

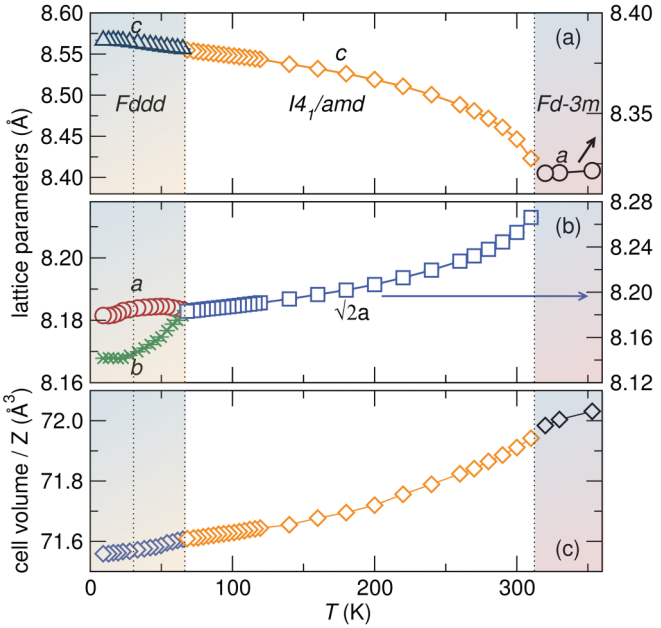

FIG. 7. (Color online) Changes in lattice parameters as a function of temperature in $NiCr_2O_4$. (a) A cubic to tetragonal structural transition occurs at 310 K where the a lattice constant of the cubic phase diverges into a and c lattice parameters of the tetragonal phase. The a lattice constant of the tetragonal cell is multiplied by $\sqrt{2}$ to clearly follow trends in the lattice parameters of $NiCr_2O_4$. In the tetragonal phase, the a parameter decreases (b) while c increases (a) with decreasing temperature. At 65 K, a tetragonal to orthorhombic structural distortion occurs resulting in three distinct lattice constants as shown in (a) and (b). (c) Variation of the cell volume normalized by the number of formula units (Z) in each cell. A further structural distortion of orthorhombic $NiCr_2O_4$ occurs at 30 K where there is a slight discontinuity of the lattice parameters (a) and (b) and cell volume (c); this is highlighted by the dashed line at $T = 30$ K. In (a), (b), and (c) the error bars are smaller than the data symbols.

a saturation magnetization of 0.725 μ_B is measured at 2 K. The measured saturation magnetization of $CuCr_2O_4$ is in good agreement with that of the triangular magnetic structure observed previously using neutron powder diffraction.[27]

The Curie-Weiss (CW) equation $\chi = C/(T - \Theta_{CW})$ is applied to paramagnetic regimes of $NiCr_2O_4$ and $CuCr_2O_4$ yielding an effective moment (μ_{eff}) of 6.53 μ_B per formula unit for $NiCr_2O_4$ and 4.27 μ_B per formula unit for $CuCr_2O_4$. The expected μ_{eff} of $NiCr_2O_4$ is 6.16 μ_B per formula unit of $NiCr_2O_4$. This value is slightly smaller that the experimentally determined value of 6.53 μ_B per formula unit obtained from fitting the paramagnetic regime to the Curie-Weiss model, implying a small orbital contribution to the measured moment. The expected μ_{eff} of 5.74 μ_B per formula unit of $CuCr_2O_4$ is much larger than the experimental value, suggesting the likely presence of magnetic correlations in the paramagnetic regime.[36] The CW temperature (Θ_{CW}) of $NiCr_2O_4$ is -487 K while that of $CuCr_2O_4$ is -147 K. The frustration index ($|\Theta_{CW}|/T_N$) of $NiCr_2O_4$ is about 7.8 and that of $CuCr_2O_4$ is 1.1, indicating that $NiCr_2O_4$ is the more frustrated compound. The negative sign of Θ_{CW} coupled with the low saturation magnetization observed in isothermal field-dependent measurements is consistent with noncollinear ferrimagnetic ordering in $NiCr_2O_4$ and $CuCr_2O_4$.

The magnetic transitions of $CuCr_2O_4$ and $NiCr_2O_4$ are strongly coupled to the lattice. All magnetic changes in $NiCr_2O_4$ are accompanied by structural transitions. The known Jahn-Teller cubic to tetragonal structural distortion in $NiCr_2O_4$ at 310 K causes a small change in the temperature-dependent magnetization [Fig. 1(a)].[12] Ishibashi and Yasumi reported further distortion from tetragonal to orthorhombic symmetry at the onset of ferrimagnetic order ($T_N = 65$ K).[12] We observe this tetragonal to orthorhombic crystal distortion occurring concurrently with the onset of ferrimagnetic order in $NiCr_2O_4$ in Fig. 4. A low-temperature anomaly at $T = 30$ K has been observed in magnetic susceptibility and heat capacity measurements of $NiCr_2O_4$; however, there is no prior report of a concurrent structural distortion.[12,13] In the current study, using high-resolution x-ray powder diffraction, we find evidence for a structural distortion at $T = 30$ K, as described in detail in a later section. Similarly, an orthorhombic distortion of the already Jahn-Teller distorted tetragonal $CuCr_2O_4$ occurs concurrently with ferrimagnetic ordering at 130 K (Fig. 5). This transition in $CuCr_2O_4$ is observed here using variable-temperature high-resolution synchrotron x-ray powder diffraction performed on a sample of crushed single crystals.

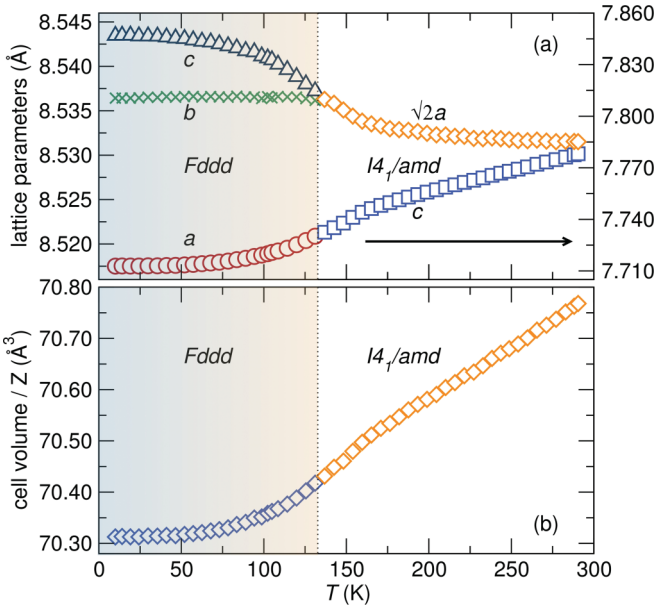

FIG. 8. (Color online) (a) The thermal evolution of lattice parameters of $CuCr_2O_4$ reveals a tetragonal $I4_1/amd$ to orthorhombic $Fddd$ structural transition at ~130 K. The tetragonal a lattice parameter has been multiplied by $\sqrt{2}$ to match the low temperature b and c lattice values of the orthorhombic $Fddd$ cell. (b) Temperature dependence of the cell volume normalized by the number of formula units (Z) in each cell shows a steady decrease with temperature. In both (a) and (b), the error bars are smaller than the data symbols.

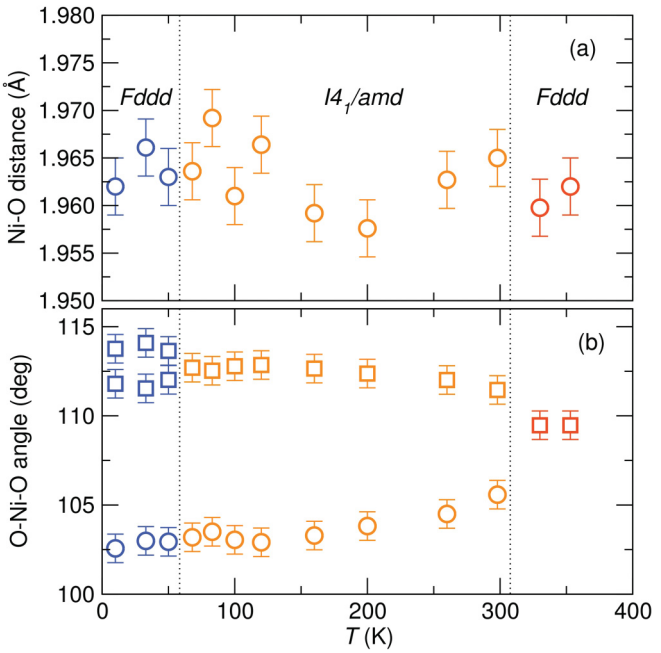

FIG. 9. (Color online) The variation in NiO_4 polyhedra as a function of temperature. (a) The Ni-O bond length remains relatively constant in all the structural phases. (b) The single O-Ni-O angle of the cubic phase separates into a larger angle and a smaller angle in the tetragonal phase. Below the orthorhombic transition, there are three distinct O-Ni-O angles.

B. Crystal structure

The ambient temperature structure of both compounds can be indexed in the tetragonal centrosymmetric space group $I4/amd$. At 298 K, $NiCr_2O_4$ is still undergoing the Jahn-Teller driven cubic-tetragonal transition and better structural parameters of the tetragonal phase are obtained at 100 K. Structural parameters obtained from Rietveld refinement of 100 K diffraction data for $NiCr_2O_4$ and 298 K diffraction data for $CuCr_2O_4$ to the space group $I4/amd$ are shown in Table I and are in good agreement with previous reports.[20,29]

Magnetic ordering drives further structural distortions in $NiCr_2O_4$ and $CuCr_2O_4$.[12,14] The low symmetry structures of $NiCr_2O_4$ and $CuCr_2O_4$ are described by the orthorhombic space group $Fddd$. $Fddd$ is a maximal nonisomorphic subgroup of $I4_1/amd$ and is derived from the parent $Fd\bar{3}m$ by loss of all threefold rotation axes and part of the twofold screw axes. Rietveld refinement fits of 10 K diffraction data to the orthorhombic space group $Fddd$ for both $NiCr_2O_4$ and $CuCr_2O_4$ are shown in Fig. 6. Symmetry lowering in $NiCr_2O_4$ and $CuCr_2O_4$ is demonstrated by the splitting of certain high symmetry diffraction peaks as illustrated in Figs. 6(c) and 6(f). The current work is the first description of the orthorhombic $Fddd$ structure for $CuCr_2O_4$. In $NiCr_2O_4$, variable-temperature synchrotron x-ray diffraction measurements show additional structural changes below 30 K, in concurrence with anomalies in specific heat and susceptibility measurements of $NiCr_2O_4$ reported both here and previously in the literature. This low-temperature structural change of $NiCr_2O_4$ is discussed in detail in a later section.

Changes in structural symmetry are reflected in the temperature dependence of lattice parameters. At 310 K there is a cubic to tetragonal transition in $NiCr_2O_4$ that splits the cubic a lattice constant into tetragonal a and c lattice parameters [Figs. 7(a) and 7(b)]. Below 310 K, the tetragonal $NiCr_2O_4$ distortion grows, with an increasing c and a decreasing a lattice constant (plotted as $\sqrt{2}a$). Below 65 K, magnetic ordering occurs concurrently with a transition to orthorhombic symmetry. The tetragonal a lattice parameter of $NiCr_2O_4$ diverges into distinct orthorhombic a and b lattice constants [Fig. 7(b)]. At 30 K, a slope change clearly visible in the a and c lattice parameters [Fig. 7] matches anomalies in other property measurements, as will be discussed later. $CuCr_2O_4$ is already tetragonal at ambient temperature due to cooperative Jahn-Teller ordering at 853 K. The tetragonal lattice constants of $CuCr_2O_4$ diverge below 300 K with c decreasing and the a lattice constant [plotted as $\sqrt{2}a$ in Fig. 8(a)] increasing, resulting in an enhanced tetragonal distortion with decreasing temperature. Below 130 K, where an orthorhombic distortion occurs concurrently with the onset of ferrimagnetic order [Fig. 8(a)], distinct a, b, and c orthorhombic lattice constants emerge. The orthorhombic lattice constants continue to diverge from 130 K to the lowest temperatures measured, as indicated in Fig. 8(a). The structural change due to orbital ordering in $NiCr_2O_4$ at 310 K results in a discontinuity of the normalized cell volume indicating a first-order phase transition. In contrast, in the low-temperature tetragonal to orthorhombic phase transitions in $NiCr_2O_4$ and $CuCr_2O_4$ the continuous slope of the normalized cell volume through the magnetostructural transition indicates a second-order phase transition [Figs. 7(c) and 8(b)].

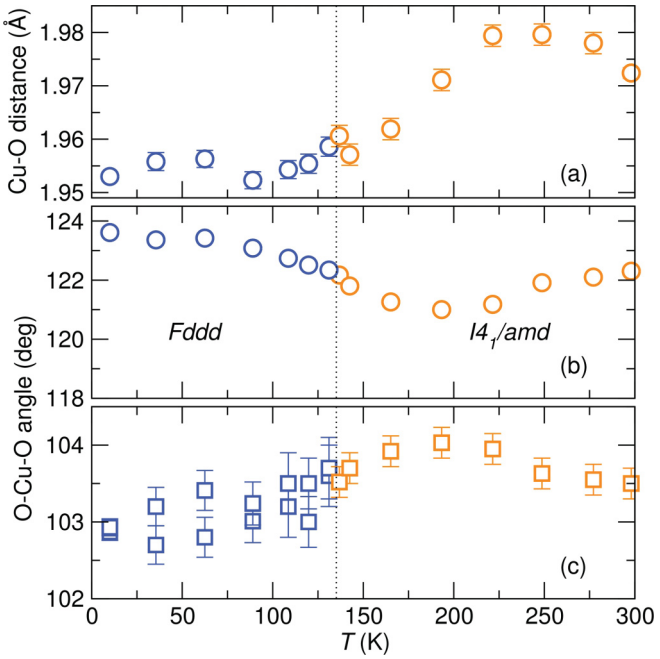

FIG. 10. (Color online) Changes in the CuO_4 polyhedra as a function of temperature. (a) There is an overall decrease in the Cu-O bond distance, (b) an increase in the larger O-Cu-O angle, and (c) a decrease in the smaller O-Cu-O angle coupled with a splitting of this angle. These trends are obtained from Rietveld refinement of synchrotron x-ray diffraction data.

Structural changes in $NiCr_2O_4$ and $CuCr_2O_4$ originate from deformations of NiO_4 and CuO_4 polyhedra. In a perfect tetrahedron, all bond lengths are equal and all O-cation-O angles are 109.5°. Ideal NiO_4 tetrahedra are observed in the cubic $NiCr_2O_4$ structure above 310 K [Figs. 9(a) and 9(b)]. Orbital ordering results in a distorted tetrahedron with a single Ni-O bond distance, but two O-Ni-O angles [Figs. 9(a) and 9(b)] in the tetragonal phase. Below 65 K, the orthorhombic structure preserves a single Ni-O bond length, but splits the O-Ni-O angles into three distinct O-Ni-O angles in the NiO_4 tetrahedra [Figs. 9(a) and 9(b)]. These distortions in Ni-O bond lengths and O-Ni-O bond angles result in an elongation of NiO_4 tetrahedra. At ambient temperature, CuO_4 tetrahedra are already significantly distorted with two different O-Cu-O angles and a single Cu-O bond distance. With decrease in temperature and the onset of the orthorhombic structural transition, we note a decrease in Cu-O bond lengths [Fig. 10(a)], an increase in the larger O-Cu-O angle [Fig. 10(b)], and a decrease in the smaller O-Cu-O angle [Fig. 10(c)]. The two smaller O-Cu-O angles divide into two. The overall effect of these structural changes is a flattening of the CuO_4 polyhedra toward a square planar configuration. The differences in the distortion of the CuO_4 and NiO_4 tetrahedra are apparent in the average low-temperature structures of $NiCr_2O_4$ and $CuCr_2O_4$ shown in Fig. 11.

C. Heat capacity

There are several interesting features in the heat capacity of $NiCr_2O_4$ and $CuCr_2O_4$ that occur concurrently with magnetic and structural transformations in these compounds. Klemme and Miltenburg report three anomalies in the heat capacity of

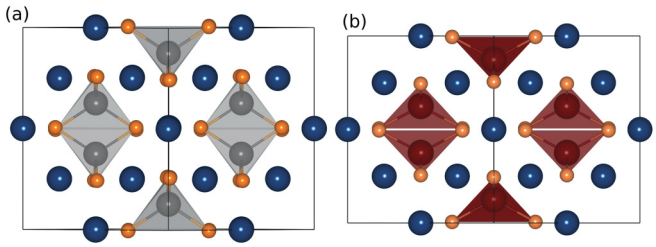

FIG. 11. (Color online) Low-temperature (10 K) orthorhombic crystal structures of (a) $NiCr_2O_4$ projected down the [101] direction and (b) $CuCr_2O_4$ projected down the [011] direction. Ni (grey) and Cu (red) are tetrahedrally coordinated by oxygen (orange). Chromium is shown in blue. The elongation of NiO_4 tetrahedra along with the compression of CuO_4 polyhedra is clearly seen in the low-temperature average structures.

$NiCr_2O_4$ occurring at 310, 75, and 30 K.[13] Our heat capacity measurements over the temperature range $3 \leqslant T \leqslant 200$ K for $NiCr_2O_4$ show two anomalies at 65 and 30 K [Fig. 12(a)]. The Jahn-Teller cubic-tetragonal structural distortion of $NiCr_2O_4$ causes the anomaly in heat capacity at 310 K reported by Klemme and Miltenburg.[13] The transition into a ferrimagnetic ordered state [Fig. 4(a)] that occurs concurrently with a structural change [Fig. 4(b)] results in the change in entropy that we observe at 65 K and was reported by Klemme and Miltenburg to occur at $T = 75$ K. Klemme and Miltenburg also reported an additional anomaly in specific heat at 30 K; Ishibashi and Yasumi noted a change in magnetic susceptibility

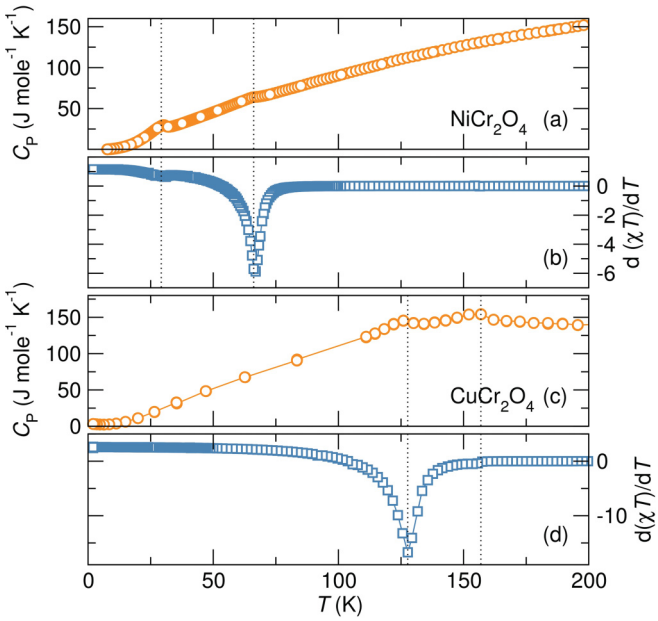

FIG. 12. (Color online) Entropy changes in $NiCr_2O_4$ and $CuCr_2O_4$ resulting from structural and magnetic transformations. (a) The heat capacity of $NiCr_2O_4$ shows two anomalies at 65 and 30 K. (b) Fisher heat capacity of $NiCr_2O_4$ indicating release of magnetic entropy occurring at the same temperatures where changes in specific heat are observed. (c) $CuCr_2O_4$ also shows two transitions in the heat capacity at 155 and 130 K. Concurrent with these changes in heat capacity of $CuCr_2O_4$ are variations in magnetic structure as illustrated by Fisher heat capacity shown in (d).

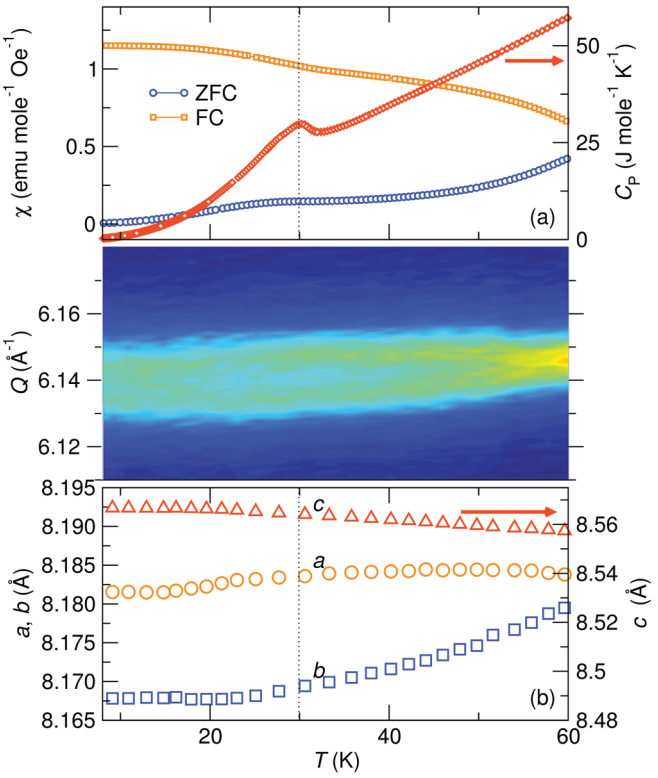

FIG. 13. (Color online) Changes in magnetic order and heat capacity of $NiCr_2O_4$ at $T = 30$ K are accompanied by a structural change. (a) Zero field cooled and field cooled temperature-dependent magnetic susceptibility measurements of $NiCr_2O_4$ show a change in magnetic order at $T = 30$ K. Concurrent with this transition in magnetism is a change in entropy indicated by the anomaly in heat capacity. The central panel tracks changes in intensity of the orthorhombic 080 and 800 reflections at $T = 30$ K illustrating that a structural change takes place at $T = 30$ K. (c) This structural change is also reflected in the temperature-dependent lattice constants of $NiCr_2O_4$ which vary at this temperature. The structural distortion above occurs in the Q range 10^{-2}Å within the instrumental resolution of 10^{-4}Å.

at this temperature.[12,13] We observe this anomaly in the heat capacity of $NiCr_2O_4$ at 30 K and attribute it to an additional change in the magnetic [Fig. 12(b)] and crystal structure [Fig. 4(b)] as will be discussed in Sec. III D of this paper.

There are two anomalies in the specific heat of $CuCr_2O_4$ at 130 and 155 K [Fig. 12(c)]. The anomaly at 130 K is coincident with ferrimagnetic [Fig. 12(d)] and tetragonal-orthorhombic [Fig. 5(b)] phase transitions in the compound. The transition into the orthorhombic ferrimagnetic state in $CuCr_2O_4$ occurs through an intermediate step with signatures in Fisher heat capacity and specific heat measurements at 155 K [Fig. 12(c) and 12(d)].[37] Slight structural effects accompany this second transition as shown in Fig. 8(b) where there is a subtle inflection point of the evolution of cell volume with temperature. Further characterization of this intermediate change in the magnetism of $CuCr_2O_4$ at about 155 K requires careful investigation in future study.

D. 30 K magnetostructural transition of $NiCr_2O_4$

During the ferrimagnetic transition of $NiCr_2O_4$, a simultaneous cooperative crystal distortion from tetragonal to orthorhombic symmetry occurs as reported by Ishibashi and Yasumi.[12,30] We observe this magnetostructural transition in $NiCr_2O_4$ at $T = 65$ K (Figs. 4 and 7). Magnetic susceptibility measurements by Ishibashi and Yasumi show yet another low-temperature magnetic transition in $NiCr_2O_4$ at $T = 31$ K that was reported by Tomitasu and Kagomiya as corresponding to the ordering of the antiferromagnetic component of the magnetic structure of $NiCr_2O_4$. Klemme and Miltenburg also observed a change in entropy at this temperature;[13] however, no changes of the average structure of $NiCr_2O_4$ have been observed at $T = 31$ K.[12,30] Our measurements reveal similar anomalies in the magnetism and specific heat measurements of $NiCr_2O_4$ [Fig. 13(a)] at $T = 30$ K. Furthermore, we observe a slight change in average structure at this temperature. The central panel in Fig. 13(b) tracks a $NiCr_2O_4$ Bragg diffraction peak as a function of temperature and shows a distinct peak narrowing and intensity change below 30 K. Likewise, the $Fddd$ lattice parameters obtained from Rietveld analysis of the variable temperature diffraction data Fig. 7 show a clear change in slope near 30 K [Fig. 13(b)]. However, no evidence for a further change of $NiCr_2O_4$ symmetry (e.g., to monoclinic) below 30 K is found in these high-resolution powder diffraction data. This structural effect is concurrent with reported anomalies in heat capacity and magnetic measurements, and will be further examined in future studies.

IV. CONCLUSIONS

Structural changes occur concurrently with magnetic phase transitions in $NiCr_2O_4$ and $CuCr_2O_4$. We have resolved details of the crystal structure of the low-temperature phase of $NiCr_2O_4$ and $CuCr_2O_4$ in the orthorhombic space group $Fddd$ and present a structural description of orthorhombic $CuCr_2O_4$. We find that the magnetic transition at 30 K in $NiCr_2O_4$ is also accompanied by further subtle structural anomaly. Pronounced elongation of NiO_4 tetrahedra and compression of CuO_4 tetrahedra toward a square planar configuration drive the distortions into the orthorhombic phase in these compounds. As postulated by Smart and Greenwald, we suggest that multiple exchange coupling pathways in the distorted orthorhombic structure are likely to be the reason behind the strong magnetostructural coupling observed in these compounds.[19] We anticipate that this study will inspire further investigation of such coupling in ferrimagnetic spinels.

ACKNOWLEDGMENTS

The 11-BM beamline at the Advanced Photon Source is supported by the Department of Energy, Office of Science, Office of Basic Energy Sciences, under Contract No. DE-AC02-06CH11357. M.C.K. thanks P. T. Barton and A. Goldman for helpful discussions. M.C.K. is supported by the Schlumberger Foundation Faculty for the Future Fellowship, and the research (M.C.K. and R.S.) is supported by the National Science Foundation through a Materials World Network grant (DMR 0909180). We acknowledge the use of shared experimental facilities of the Materials Research Laboratory: an NSF MRSEC, supported by NSF DMR 1121053. The M.R.L. is a member of the NSF-supported Materials Research Facilities Network (www.mrfn.org).

*suchomel@aps.anl.gov
†dshoemaker@anl.gov
‡ribaud@anl.gov
§kemei@mrl.ucsb.edu
‖seshadri@mrl.ucsb.edu

[1]J. Dunitz and L. Orgel, J. Phys. Chem. Solids **3**, 20 (1957).
[2]G. Beni and P. Pincus, J. Chem. Phys. **57**, 3531 (1972).
[3]X. Fabreges, S. Petit, I. Mirebeau, S. Pailhes, L. Pinsard, A. Forget, M. T. Fernandez-Diaz, and F. Porcher, Phys. Rev. Lett. **103**, 067204 (2009).
[4]S. Lee, A. Pirogov, M. Kang, K.-H. Jang, M. Yonemura, T. Kamiyama, S.-W. Cheong, F. Gozzo, N. Shin, H. Kimura *et al*., Nature **451**, 805 (2007).
[5]T. Lottermoser, T. Lonkai, U. Amann, D. Hohlwein, J. Ihringer, and M. Fiebig, Nature **430**, 541 (2004).
[6]V. N. Glazkov, A. M. Farutin, V. Tsurkan, H.-A. Krug von Nidda, and A. Loidl, Phys. Rev. B **79**, 024431 (2009).
[7]H. Ueda, H. A. Katori, H. Mitamura, T. Goto, and H. Takagi, Phys. Rev. Lett. **94**, 047202 (2005).
[8]O. Tchernyshyov, Phys. Rev. Lett **93**, 157206 (2004).
[9]T. Rudolf, C. Kant, F. Mayr, J. Hemberger, V. Tsurkan, and A. Loidl, New J. Phys. **9**, 76 (2007).
[10]C. Kant, J. Deisenhofer, V. Tsurkan, and A. Loidl, J. Phys. Conf. Ser. **200**, 032032 (2010).
[11]S.-H. Lee, G. Gasparovic, C. Broholm, M. Matsuda, J. Chung, Y. Kim, H. Ueda, G. Xu, P. Zschack, K. Kakurai *et al*., J. Phys. Condens. Matter **19**, 145259 (2007).
[12]H. Ishibashi and T. Yasumi, J. Magn. Magn. Mater. **310**, e610 (2007).
[13]S. Klemme and J. van Miltenburg, Phys. Chem. Miner. **29**, 663 (2002).
[14]S. Bordacs, D. Varjas, I. Kezsmarki, G. Mihaly, L. Baldassarre, A. Abouelsayed, C. A. Kuntscher, K. Ohgushi, and Y. Tokura, Phys. Rev. Lett. **103**, 077205 (2009).
[15]S. Greenwald, Nature **168**, 379 (1951).
[16]J. Smart and S. Greenwald, Phys. Rev. **82**, 113 (1951).
[17]W. Roth, Phys. Rev. **110**, 1333 (1958).
[18]Y. Li, Phys. Rev. **100**, 672 (1955).
[19]J. Smart and S. Greenwald, Nature **166**, 523 (1950).
[20]O. Crottaz, F. Kubel, and H. Schmid, J. Mater. Chem. **7**, 143 (1997).
[21]K. Ohgushi, Y. Okimoto, T. Ogasawara, S. Miyasaka, and Y. Tokura, J. Phys. Soc. Jpn. **77**, 034713 (2008).
[22]Z. Ye, O. Crottaz, F. Vaudano, F. Kubel, P. Tissot, and H. Schmid, Ferroelectr. Lett. **162**, 103 (1994).
[23]Y. Chukalkin, V. Petrov, V. Shtirts, and B. Goshchitskii, Phys. Status Solidi A **92**, 347 (1985).
[24]J. Kanamori, J. Appl. Phys. **31**, S14 (1960).
[25]M. Gerloch, Inorg. Chem. **20**, 638 (1981).
[26]M. Tovar, R. Tobari, C. Welker, and F. Fleischer, Phys. B: Conden. Matt. **385**, 196 (2006).
[27]E. Prince, Acta Cryst. **10**, 554 (1957).
[28]W. Dollase and H. O'Neill, Acta Crystallogr. Sect. C **53**, 657 (1997).
[29]G. Ueno, S. Sato, and Y. Kino, Acta Crystallogr. Sect. C **55**, 1963 (1999).
[30]K. Tomiyasu and I. Kagomiya, J. Phys. Soc. Jpn. **73**, 2539 (2004).
[31]J. Wang, B. H. Toby, P. L. Lee, L. Ribaud, S. M. Antao, C. Kurtz, M. Ramanathan, R. B. von Dreele, and M. A. Beno, Rev. Sci. Instrum. **79**, 085105 (2008).
[32]B. Toby, J. Appl. Crystallogr. **34**, 210 (2001).
[33]A. C. Larson and R. B. Von Dreele, "General Structure Analysis System (GSAS)", Los Alamos National Laboratory Report LAUR 86-748 (2000).
[34]K. Momma and F. Izumi, J. Appl. Crystallogr. **41**, 653 (2008).
[35]B. C. Melot, J. E. Drewes, R. Seshadri, E. M. Stoudenmire, and A. P. Ramirez, J. Phys. Condens. Matter **21**, 216007 (2009).
[36]M. Kemei, S. Moffitt, D. Shoemaker, and R. Seshadri, J. Phys. Condens. Matter **24**, 046003 (2012).
[37]M. Fisher, Philos. Mag. **7**, 1731 (1962).